LCL Filter Grid Connected Inverter with Harmonics Modeling Flexibility

Marcelo Piveta * **Emerson G. Carati** * **Jean P. da Costa** *

* *Programa de Pós-Graduação em Engenharia Elétrica*
Universidade Tecnológica Federal do Paraná, PR.
(e-mail: marcelopiveta@alunos.utfpr.edu.br).
(e-mail: emerson@utfpr.edu.br).
(e-mail: jpcosta@utfpr.edu.br)

Abstract: In the last decades, distributed generation (DG) has experienced ever high growth. Most of the energy sources used in DG, notably solar and wind power, are dependent on electronic converters for integration with the main grid. The development of converters and their control structures usually applies computational simulations, which allow for fast analysis of the prototypes. However, the performance of those simulations is dependent on the model used. Grid-connected converters, like LCL-type inverters, tend to need high-order models to correctly represent most of its dynamics, which may lead to time-consuming analysis and simulations. In the literature, many works present simplified models of grid-tied inverters, being some of those unable to deal with frequency components other than the fundamental. This paper proposes a new model for an LCL filter-based grid-tied inverter with harmonics modeling flexibility, which allows the complexity to be adjusted to some extent. The considered system and its respective control scheme are firstly presented. Then, the contribution of this work is discussed for the considered study case. The main goal of this work is an approach suitable for a wide range of applications and analyses with various degrees of complexity in the field of LCL-type inverter studies. Simulation results applying the proposed model are presented and compared with results obtained via real-time domain emulations (RTDE).

Keywords: Distributed generation, Inverter, Model validation, Time-invariant systems, Simulation, Hardware-in-the-loop simulation.

1. INTRODUCTION

Distributed power generation is growing rapidly in the last decade. One of the major contributing factors is the expansion of renewable power sources, mainly solar and wind power. The energy generated by those sources is unsuitable to be directly dispatched to the main grid (Teodorescu et. al, 2011). The connection of renewable energy-based DG units to the main grid is usually done via power electronic converters, which processes the generated energy, adapting its characteristics to the grid requirements (Liston Júnior et al., 2018). One of the most widely used power converters for grid-tied DG applications is the LCL filter-based inverter. This converter can achieve high AC energy quality and presents good performance with relatively low complexity (Sayed et al., 2014). Fig. 1 shows the schematic representation of a basic DG LCL inverter-based unit.

To extract the maximum potential of the DG system, the control structures and circuit components of the converter need to be properly designed. This process usually involves defining a representative model of the system, used in computational simulations. Complex models tend to give more accurate results, representing high-frequency phenomena and non-linear dynamics. However, the analysis process is more complicated and the simulations can be time-consuming. Models like these are best suited for tasks like controller validation, stability analysis, etc (Jiang et al., 2018). On the other hand, simpler models allow for faster simulations, but generally lack precision in representing some dynamics of the system, being better suited for analysis where some of the dynamics are not relevant (Ahmad et. al, 2019).

In the case of the grid-tied LCL inverter, numerous models are discussed in the literature. One of the most important aspects of choosing an adequate model is defining which dynamics must be represented. Hu et al. (2021) and Fouladfar et al. (2021) treat the DG system as a controlled power source. This representation covers only some of the slowest dynamics of the LCL inverter, like the power dispatch, allowing for fast simulations with minimal computational burden. In contrast, Osorio et al. (2019) and Le et al. (2021) present models contemplating complex dynamics of the DG system, like LCL inductor saturation and parameter uncertainty. Models such as these contemplate high-frequency dynamics, needing small time steps in simulations. This can restrict the analysis interval and the number of DG units considered.

⋆ This study was financed in part by the Coordenação de Aperfeiçoamento de Pessoal de Nível Superior – Brasil (CAPES) – Finance Code 001. The authors also thanks FINEP, SETI, CNPq, Fundação Araucária, COPEL and UTFPR/PPGEE-PB for additional support and funding.

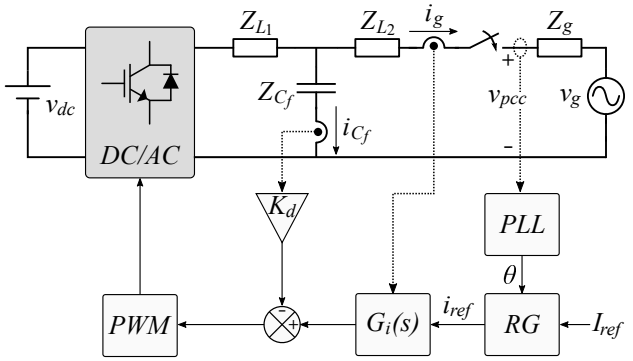

Fig. 1. Diagram of the DG unit with its respective control structure.

One of the most popular models for LCL inverters is employed by Mahlooji et al. (2018) and Wang et al. (2010), being a linear representation of the system in the frequency domain. This approach takes into account most of the LCL inverter dynamics, being well suited for applications like controller and filter design, etc (Kraemer et al., 2018). Although the model structure allows for analyzing higher frequency phenomena, some of its causes are not usually considered, like the switching of the inverter, which leads to higher-order harmonics not being generated.

Components such as LCL filter resonance and switching harmonics are relevant for many studies of energy quality and stability analysis (Han et al., 2019). As the basic linear model is somewhat insufficient to represent those dynamics, this paper proposes a modification in the model structure shown in Yang et al. (2013) that allows for flexible modeling of the higher frequency components. The fundamental component is treated like in the basic model. The main contribution of the proposed model is related to the harmonic components, which are treated as an secondary adjustable input. The proposed method allows the adaptation of the analysis detailing based most on the adjustment of the harmonic content. Numerical and real-time results are presented to analyze and demonstrate the effectiveness of the proposed approach.

The next sections of this paper are organized as follows. The DG system circuit and control structure considered as the base case are presented in Section II. Based on the referred DG system, the proposed modeling is discussed in Section III. Results obtained utilizing the proposed model and via RTDE are presented and compared in Section IV to evaluate the proposed methodology. In Section V, the conclusions of the paper are debated.

2. GRID-TIED LCL INVERTER CIRCUIT AND CONTROL STRUCTURE

Fig. 1 shows the base case of an LCL inverter-based DG unit for this paper. v_{dc} source represents the DC bus of the DG unit, treated as an ideal DC voltage source. DC/AC block is the inverter, responsible for converting the DC energy from the local source to AC. The impedances Z_{L_1}, Z_{C_f} and Z_{L_2} comprise the LCL filter, given by

$$Z_{L_1} = R_1 + sL_1 \quad , \tag{1}$$

$$Z_{C_f} = \frac{1}{sC_f} + R_{C_f} \tag{2}$$

and

$$Z_{L_2} = R_2 + sL_2 \quad , \tag{3}$$

wherein R_n and L_n $(n = 1, 2)$ are, respectively, the resistances and inductances of the inductors and C_f the filter's capacitance. Z_g and v_g are, respectively, the impedance and source of the Thevenin equivalent of the main grid, being Z_g given by

$$Z_g = R_g + sL_g \quad . \tag{4}$$

Still concerning Fig. 1, the adopted control structure is based on Kraemer et al. (2018). The PLL synchronizes the DG unit to the main grid, obtaining the angle (θ) and frequency of the voltage at the common coupling point (v_{pcc}) (Hamed et al., 2017). The angle is applied in the reference generator (RG) in addition to the current amplitude reference (I_{ref}) to obtain the reference current (i_{ref}), given by

$$i_{ref} = I_{ref} \angle \theta \quad . \tag{5}$$

The reference current is then compared to the grid injected current (i_g), resulting in an error signal applied to the current controller $(G_i(s))$. In addition to the main control loop, an active damping (AD) term is used for stability improvement. The chosen AD structure is the capacitor current (i_{C_f}) proportional feedback, whose gain (K_d) is obtained as presented by Liston Júnior et al. (2018). The resulting control signal is applied to the inverter switches via pulse-width modulation (PWM) (Holtz, 1992).

In a DG system like the discussed, dynamics around and above the fundamental frequency are relevant for power quality and stability studies. Some elements, although, such as the PLL and reference generator normally show negligible effects above the fundamental grid frequency. The AD loop, PWM, and LCL filter, on the other hand, present significant dynamics on higher frequencies (Cavazzana et al., 2018). The main control loop can also present higher frequency dynamics depending on the controller and auxiliary structures (Zammit et al., 2014).

The modulation strategy is one of the main factors that influence the harmonic content of the inverter output voltage, which is filtered by the LCL circuit (Khan et al., 2020). These harmonics are partially reflected in the grid injected current, whose total harmonic distortion (THD) is limited by standards (IEEE, 2018). Moreover, excesses in the current harmonic content can cause other problems, such as oscillations and instability (Yoon et al., 2014). Other relevant sources of high-frequency disturbances that impact current THD are grid voltage harmonics and DC bus oscillations (Baburajan et al., 2021).

A DG unit with components like the aforementioned can be represented by its linearized model, shown in Fig. 2(a) (except by the term $h(s)$, which is discussed in the following section). $G_c(s)$ is the transfer function of the modulation and inverter, usually considered as a gain and a delay (He et al., 2019). Using this representation, it is possible to take into account the harmonic components of

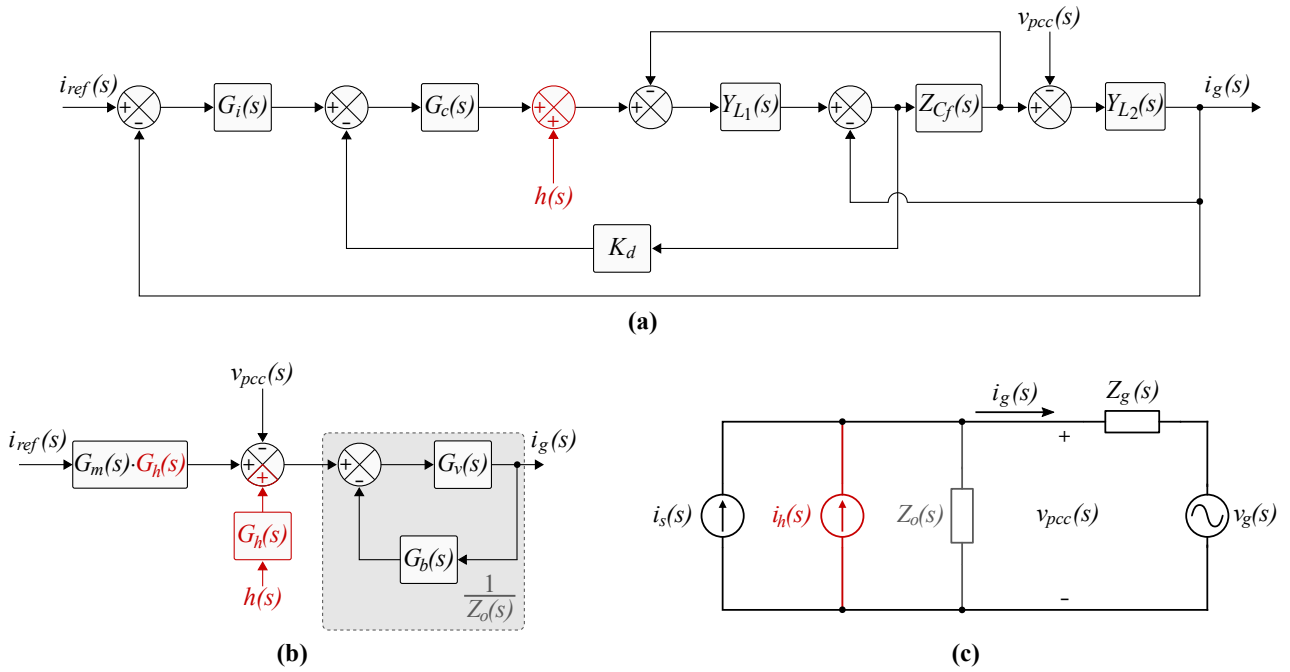

Fig. 2. (a) Complete block diagram of DG system. (b) Reduced block diagram with output impedance in evidence. (c) Norton equivalent. In red, the proposed modification. Based in Yang et al. (2013).

v_{pcc} and DC bus oscillations. The harmonics introduced by the PWM, however, are not usually represented.

3. FLEXIBE HARMONICS MODELING

Given the relevant impact of the modulation on the overall energy quality and stability, representing the added high-frequency components into the model can be useful. Those harmonics are generated in the output voltage of the inverter and propagated to the voltages and currents of the LCL filter, although in a smaller amplitude due to attenuation (Shireen, Kulkarni, 2003). In this sense, a modification in the base linearized model of the grid-tied LCL-type inverter is proposed, with the addition of the term $h(s)$, shown in Fig. 2(a). The term $h(s)$ is an input signal which accounts for the harmonic content inserted by the PWM.

Realizing the simplification in the block diagram of Fig. 2(a), it can be reduced to the shown in Fig. 2(b). Similar approaches are presented in the literature for the base linearized model (Yang et al., 2014). The blocks in Fig. 2(b) are given by

$$G_m(s) = G_i(s)G_p(s) \ , \tag{6}$$

$$G_h(s) = \frac{Y_{L_1}(s)Z_{C_f}(s)}{Y_{L_1}(s)(Z_{C_f}(s) + K_d G_p(s)) + 1} \ , \tag{7}$$

$$G_v(s) = Y_{L_2}(s) \ , \tag{8}$$

and

$$G_b(s) = \frac{Z_{C_f}(s)(1 + G_i(s)G_p(s)Y_{L_1}(s))}{1 + Y_{L_1}(s)(Z_{C_f}(s) + K_d G_p(s))} \ . \tag{9}$$

In (7)-(9), the admittance terms are

$$Y_{L_1}(s) = \frac{1}{Z_{L_1}(s)} = \frac{1}{R_1 + sL_1} \tag{10}$$

and

$$Y_{L_2} = \frac{1}{Z_{L_2}(s)} = \frac{1}{R_2 + sL_2} \ . \tag{11}$$

The equivalent output admittance of the DG unit seen from the grid $(1/Z_o(s))$ is highlighted in Fig. 2(b). Using this parameter, it is possible to obtain the modified Norton equivalent of the DG unit shown in 2(c). This representation is interesting as can be easily used for stability analysis of individual or multiple inverters (Cavazzana et al., 2018). The expressions for the current sources of the modified Norton equivalent are

$$i_s(s) = \frac{G_m(s)G_h(s)G_v(s)}{1 + G_v(s)G_b(s)} \cdot i_{ref}(s) \tag{12}$$

$$i_h(s) = \frac{G_h(s)G_v(s)}{1 + G_v(s)G_b(s)} \cdot h(s) \tag{13}$$

and for the output impedance of the DG unit seen from the grid

$$Z_o(s) = Y_o(s)^{-1} = \frac{1 + G_v(s)G_b(s)}{G_v(s)} \ . \tag{14}$$

Analyzing the circuit shown in Fig. 2(c), the current injected into the grid by the DG unit can be obtained as

$$i_g(s) = i_s(s) + i_h(s) - i_z(s) \ , \tag{15}$$

wherein

$$i_z(s) = \frac{1}{Z_o} \cdot v_{pcc}(s) \quad . \tag{16}$$

The term $h(s)$ can also be used to insert additional perturbations to the system, such as harmonics near the resonance frequency of the LCL filter. As presented by Zhang et al. (2006), the frequency spectrum of the output voltage of an inverter controlled via PWM is composed of a fundamental component (at frequency f) and infinite sidebands of high-frequency components, centered around integer multiples of the switching frequency (f_s). Fig. 3 shows a generic pattern of components for the output voltage of a PWM-driven inverter. It is important to emphasize that the exact spectrum depends on many factors, such as the type of PWM applied (Mouton et al., 2012).

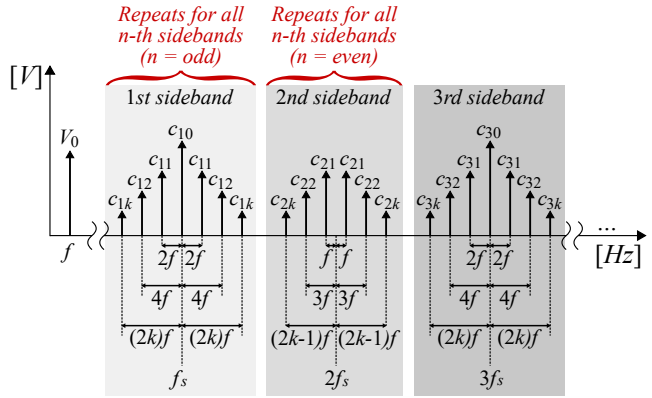

Fig. 3. Generic harmonic spectrum of the output voltage of an PWM-driven inverter. Based in Zhang, 2006.

In Fig. 3, c_{nk} are the amplitude of the harmonics, being n the order of the switching harmonic and k the number of the sideband. The amplitude of the introduced component is inversely proportional to its frequency, as discussed by Du et al. (2013). Because of this attenuation, the higher-order sidebands generally do not produce any significant impact. The first ones, on the other hand, influences heavily the performance of the inverter (Yang et al., 2017).

The fundamental component of the output voltage (V_0) in Fig. 3 is present in both the basic linearized and proposed models. However, the content of the sidebands is only represented in the second. In the Norton equivalent shown in Fig. 2(c), $i_s(s)$ generates the current caused by V_0 while $i_h(s)$ generates the current by all the considered harmonic components combined. In fact, it can be noted in Fig. 2(a) that if the input $h(s)$ is set to zero, the proposed model is equivalent to the traditional linearized one. The separation between $i_s(s)$ and $i_h(s)$ contributions to $i_g(s)$, for a generic harmonic content $h(s)$ based on the shown in Fig. 3 is observed in Fig. 4.

As can be seen in Fig. 4, the contributions of $i_s(s)$ to $i_g(s)$ is composed almost entirely of a fundamental component. This behavior is expected as $i_s(s)$ is caused only by the fundamental voltage component. $i_h(s)$ is comprised mainly of harmonics at frequencies around the sidebands caused by the PWM. The effect of the filtering can be noted on the

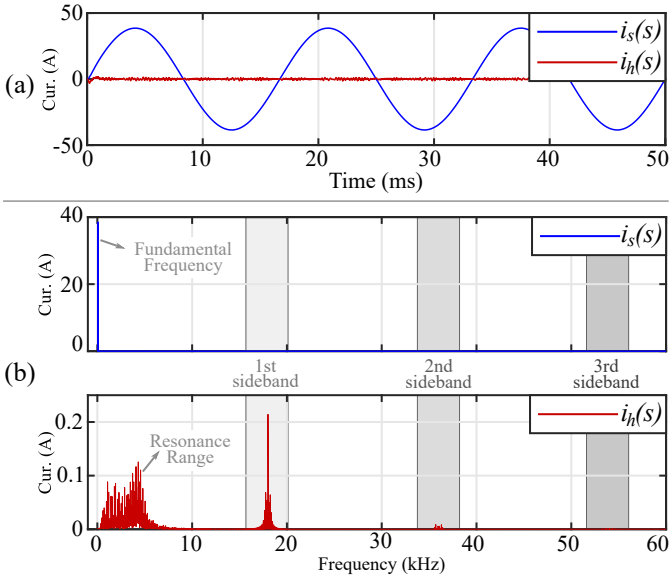

Fig. 4. Contributions of $i_s(s)$ and $i_h(s)$. (a) Time domain. (b) Frequency Spectrum.

frequency spectrum of $i_h(s)$. Components with frequencies above the first sideband get severely attenuated.

Moreover, significant components near the LCL filter resonance range (around $2-5kHz$) are present, although $h(s)$ does not have any harmonics in this range. The presence of those components is caused by the terms of (13) which are related to the LCL filter impedances. In fact, $i_s(s)$ also has components in this frequency range, but are considerably smaller than the main component, being negligible.

For obtaining $i_g(s)$, it is necessary to account for the effects of $Y_o(s)$. The current $i_z(s)$ is dependent on $v_{pcc}(s)$, which in turn is influenced by both v_g and $i_s(s) + i_h(s)$. In this sense, the output impedance (or admittance) can be seen as the interface between the grid and the DG unit. Due to this characteristic, as shown by Ray (2021), the stability of a grid-tied DG unit is determined by $Y_o(s)$. The transfer function (14) contains terms related to the current controller, LCL filter impedances, and AD structure. Although all of those elements impact the stability of the system, the AD usually is the most critical. Fig. (5) shows the poles and zeros and the Bode diagrams of (14) for a range of values of K_d.

In Fig. 5(a), the red arrows indicate the trajectory of the poles of $Y_o(s)$ as the value of K_d increases. It can be noted that the AD structure is essential for the stability of the system. Without damping ($K_d = 0$), a pair of poles of the system is located in the instability region. The same occurs if the damping coefficient is insufficient. As K_d increases, all the poles are allocated inside the stability region. The system also presents poles near the origin, but are either canceled with zeros or relatively insensitive to changes in K_d. Similar analysis can be made varying other parameters of the system, such as controller gains. In this sense, it becomes clear that the model for $Y_o(s)$ is sufficient for analyzing and representing the DG system stability.

The effect of the pole movement in the frequency response of $Y_o(s)$ can be seen in Fig. 5(b). The major impact of AD is in the resonance range, where the negative peak

gain caused by the LCL filter occurs. For higher values of K_d, the negative peak is severely attenuated. In addition, the phase transition becomes smoother. This change in the frequency response is related to the movement of the poles towards the stability region. The poles of $Y_o(s)$ which are inside the stability region even without AD do not cross for the instability region, but are moved towards the real axis.

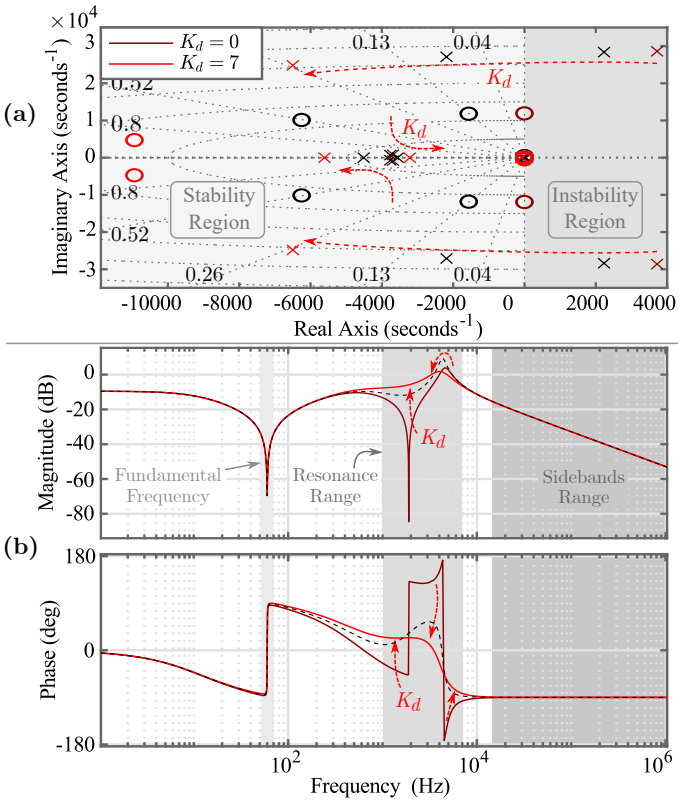

Fig. 5. $Y_o(s)$ behavior for a range of K_d. (a) Poles and zeros. (b) Bode diagrams. In black: intermediate values of K_d for better visualization of the trajectory.

It is important to notice that the effect of AD is predominantly around the resonance range. Fig 5(b) shows that for the fundamental frequency and the sidebands range (high-frequency components), the response of $Y_o(s)$ does not change significantly with the increase of K_d. The fundamental component presents a high negative gain, caused by the current controller. This indicates that most of the generated current at this frequency is injected into the grid. Similarly, $Y_o(s)$ also presents low admittance for high-frequency components. By this behavior, most of the content of $i_h(s)$ is present in $i_g(s)$.

4. DISCUSSION AND RESULTS ANALYSIS

To validate the proposed model, simulation and RTDE results are shown and compared with the ones of a more accurate switched model of an LCL-based grid-tied inverter, which is based on Fig. 1. The proposed model is implemented using (12) - (16). The parameters for both models are shown in Table I. The applied modulation is the three-level SPWM and the current controller is the non-ideal proportional-resonant (PR) (Liston Júnior et al., 2018), which transfer function is

$$G_i(s) = K_p + \frac{2K_r\omega_c s}{s^2 + 2\omega_c s + (2\pi f)^2} \quad . \tag{17}$$

Table 1. System parameters.

Parameter	Value	Parameter	Value
Grid frequency (f)	60 Hz	DC bus voltage (v_{dc})	420 V
Grid RMS voltage (v_g)	220 V	Switching frequency* (f_s)	20 kHz
Inverter side inductance (L_1)	320 μH	Rated DG power	6 kW
L_1 inductor resistance (R_1)	12 mΩ	Proportional PR gain (K_p)	3
Grid side inductance (L_2)	70 μH	Resonant PR gain (K_r)	3000
L_2 inductor resistance (R_2)	7 mΩ	PR cut-off frequency (ω_c)	1 rad/s
LCL filter capacitance (C_f)	22 μF	AD feedback gain (K_d)	7

4.1 Simulation results

For initial validation of the proposed model, a comparison between it, the basic linear model, and a switched numerical model is made via simulations in the software *PSIM*. The basic model is implemented using a block diagram, similar to Fig. 2(a). The switched model is built using the components in the software library. The proposed model is implemented in C language using the discrete versions of equations (12) - (16). Fig. 6 shows the comparison of the output current of the DG unit (i_g) in steady-state for the three considered models.

It can be seen in Fig. 6 that the resulting current for the three models is coherent. As shown in the highlighted frame, although, the basic model presents almost no oscillations. The proposed and switched models, on the other hand, present components other than the fundamental. Also, the oscillations present in these models are different. It is noticeable that the switched model presents a higher amplitude in the oscillations. For a better understanding of the characteristics of the harmonics present in the models, Fig. 7 shows the frequency spectrum of the waves of Fig. 6.

Analysing Fig. 7, it is noticeable that the proposed model carries a more significant harmonic content than the basic model. The fundamental component is similar for the three models. In the highlighted frames, it can be seen that the proposed model has a higher harmonic content than the basic one, but its characteristic is different from the switched model. The proposed model underrepresents the low-frequency components whilst overestimates the

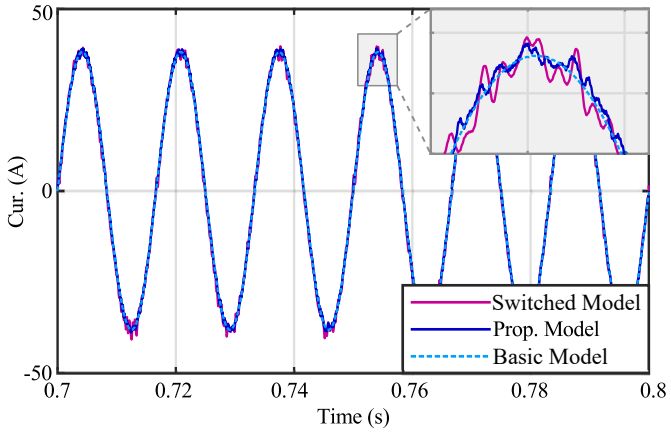

Fig. 6. Simulation results of the output current of the DG unit for different models.

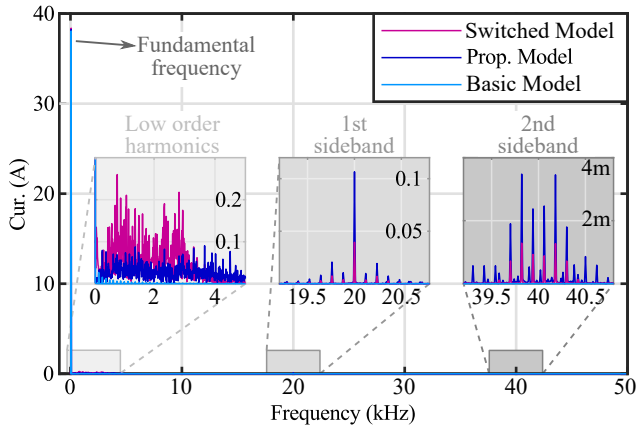

Fig. 7. Frequency spectrum of the output current of the DG unit for different models.

components of the sidebands, justifying the difference in the oscillations shown in Fig.6.

Even though the harmonic content still different from the switched representation, the proposed model is more accurate than the basic model. In fact, it can be seen in Fig. 7 that some components that are represented by the proposed model are absent for the simpler one. The calculated THDs for i_g in the scenario of Fig. 6 are 0.15%, 1.98%, and 3.42% for, respectively, the basic, proposed and switched models. In this sense, it becomes clear that the proposed model is an intermediate approximation of the real DG system.

4.2 RTDE results

For further validation of this paper's contribution, RTDE simulations are performed. Figure 8 shows the RTDE setup used to obtain the results.

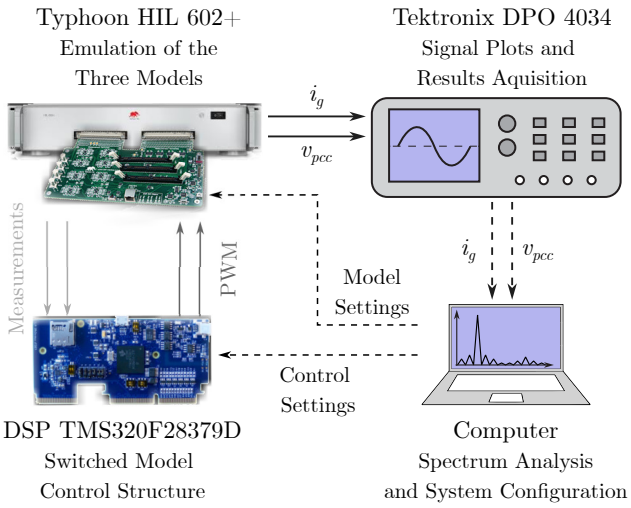

Fig. 8. RTDE Setup. Continuous lines represent analog signals and dashed lines represent digital signals.

The RTDE allows the comparison of the proposed model with a more accurate representation of the DG unit, as it takes into account phenomena related to the digital processing of the control structure of the system. The reference results are obtained using the setup shown in Figure 8, comprised of a *Typhoon HIL* 602+ for emulating the power electronics and a *Texas Instruments* TMS320F28379D for executing the control scheme. The waveforms are captured using a *Tektronix* DPO 4034 oscilloscope. The proposed and basic models are also implemented in *Typhoon HIL* 602+. Fig. 9 shows the RTDE results of the analysis analogous to those shown in Fig. 6.

As can be seen in Fig 9(a), the results obtained for both models are very similar (the basic model results are shown just for comparison and on a different scale for better visualization). Fig. 9(b) shows the output current in another time scale for better visualization of the oscillations. For further analysis of the harmonics of the output current, Fig. 10 shows the frequency spectrum of the waveforms of Fig. 9.

Due to limitations of signal generation capability in the simulation hardware, $h(s)$ is simplified in the analysis of Fig. 10 in comparison to Fig. 7, consisting of only some components of the first sideband. Numerical comparisons can not be directly made. However, it can be noted that the behavior of the harmonics in the highlighted ranges is similar to that obtained in simulations. The sideband harmonics are higher in the proposed model than in the RTDE one. Inverse behavior happens for the low-order harmonics. The voltage of the common coupling point is also affected by the harmonic content of i_g, as shown in Fig. 11.

The effect of the harmonics of i_g over v_{pcc} can be noted in Fig. 11. The grid voltage (v_g) is composed only of

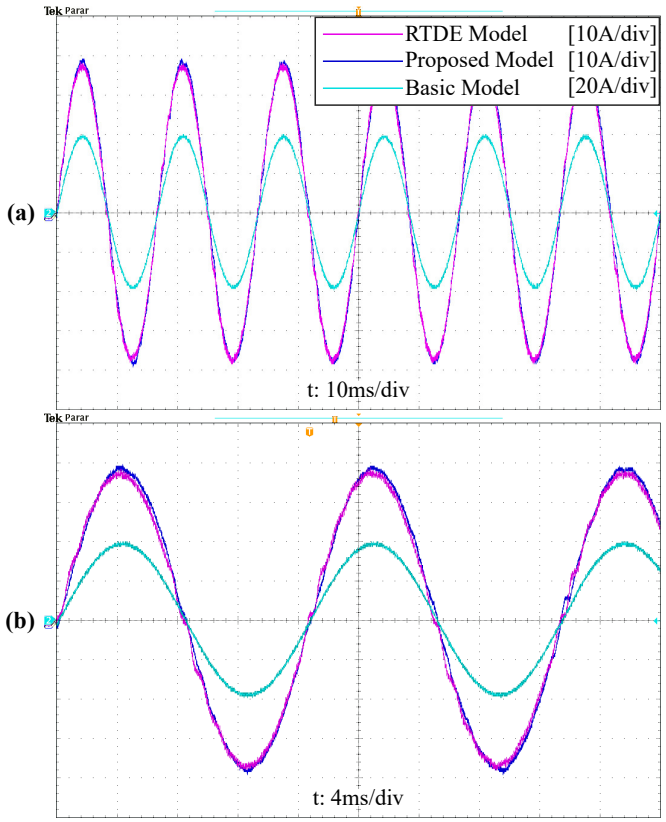

Fig. 9. RTDE results of the output current of the DG unit for different models. (a) Overall view. (b) Detail for better visualization of the harmonics.

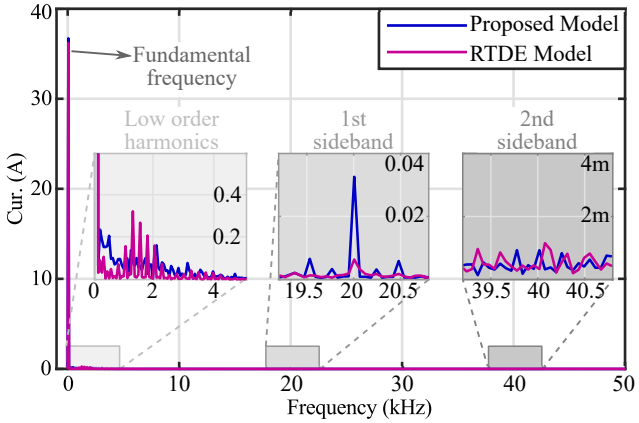

Fig. 10. Frequency spectrum of the output current of the DG unit for RTDE results.

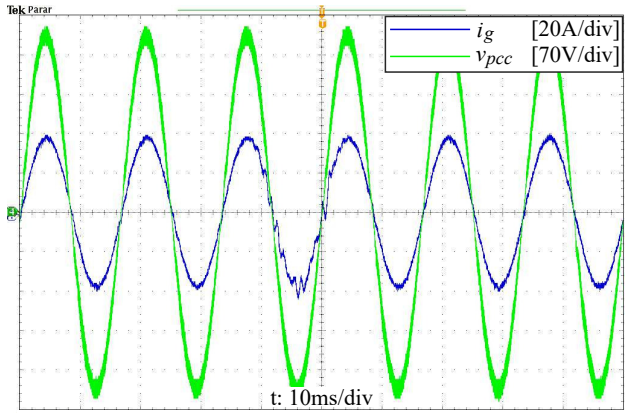

Fig. 11. Results of the output current of the DG unit and the voltage at the common coupling point.

a fundamental component, so, the high-frequency ripple present at v_{pcc} is caused by the DG unit. In this sense, it becomes clear that the proposed model can represent the coupling of the DG system and the main grid. Moreover, the equations of the model are dependent on v_{pcc}, which causes the feedback of the introduced voltage ripple in the DG unit equations. This effect is not evident in the equations of the model (although it exists in real systems), but, even with its introduction, the DG system operates correctly, maintaining stability.

Fig. 11 also shows some oscillations in i_g, which are caused by an disturbance added to i_h (addition of a small component at the resonance frequency). It is interesting to note that even with the occurrence of this perturbation the DG unit maintains stable operation and the oscillations rapidly fade out. This shows that the DG system has some robustness to disturbances, indicating the correct representation of the current control and active damping structure.

5. CONCLUSION

This paper proposes and discusses a modification in the transfer function-based model of the grid-tied LCL inverter. The proposed improvement consists of the addition of a new input signal in the model, allowing for representing the dynamics of the higher-order harmonics caused by the switching characteristic of the power converter. The main conclusions of this paper are:

- The addition of the proposed modification, the signal $h(s)$, in the LCL inverter model allows the representation of dynamics that are not contemplated by the basic model while maintaining the linearity;
- The proposed model is sufficient for impedance-based stability analysis since it takes into account the dynamics of the LCL filter, current control, and damping;
- Low order harmonics (below the resonance frequency of the LCL filter) are underrepresented and the sidebands are overestimated when compared to the more precise models;
- The proposed representation of the DG system presented an error in the THD of 1.44%, while the basic model presented an error of 3.27%. In this sense, the results show that the proposed model can take into account a wider range of dynamics present in DG units and, although not exact, is sufficient for an approximation;

REFERENCES

[1] Ahmad I, Fandi G, Muller Z, Tlusty J. (2019). Voltage Quality and Power Factor Improvement in Smart Grids Using Controlled DG Units. *Energies*. 12(18):3433. https://doi.org/10.3390/en12183433

[2] Baburajan, S., Wang, H., Kumar, D., Wang, Q., and Blaabjerg, F. (2021). DC-Link Current Harmonic Mitigation via Phase-Shifting of Carrier Waves in Paralleled Inverter Systems. *Energies*. 14, 4229. https://doi.org/10.3390/en14144229

[3] Cavazzana, F., Caldognetto, T., Mattavelli, P., Corradin, M., and Toigo, I. (2018). Analysis of Current Control Interaction of Multiple Parallel Grid-Connected Inverters. *IEEE Transactions on Sustainable Energy*. vol. 9, no. 4, pp. 1740-1749, Oct. 2018, doi: 10.1109/TSTE.2018.2811505.

[4] Du, Y., Lu, D., James, G., Cornforth, D. (2013). Modeling and analysis of current harmonic distortion from grid connected PV inverters under different operating conditions. *Solar Energy*. volume 94. 182-194. 10.1016/j.solener.2013.05.010.

[5] Fouladfar, M.H., Saeed, N., Marzband, M., and Franchini, G. (2021). Home-Microgrid Energy Management Strategy Considering EV's Participation in DR. *Energies*. 14, 5971. https://doi.org/10.3390/en14185971

[6] Hamed, H. A., Abdou, A. F., Bayoumi, E., and El-Kholy, E. E. (2017). Effective design and implementation of GSSPLL under voltage dip and phase interruption. *The Institution of Engineering and Technology Power Electronics Journal*. Vol 11. Iss 6. pp. 1018-1028.

[7] Han, Y., Yang, M., Li, H., Yang, P., Xu, L., Coelho, E., and Guerrero, J. (2019). Modeling and Stability Analysis of LCL-Type Grid-Connected Inverters: A Comprehensive Overview. *IEEE Access*. vol. 7, pp. 114975-115001, 2019, doi: 10.1109/ACCESS.2019.2935806.

[8] He, Y., Wang, X., Ruan, X., Pan, D., Xu, X., and Liu, F. (2019). Capacitor-Current Proportional-Integral Positive Feedback Active Damping for LCL-Type Grid-Connected Inverter to Achieve High Robustness Against Grid Impedance Variation.

IEEE Transactions on Power Electronics. 1–1. doi:10.1109/tpel.2019.2906217.

[9] Holtz, J. (1992). Pulsewidth modulation-a survey. *IEEE Transactions on Industrial Electronics* vol. 39, no. 5, pp. 410-420, Oct. 1992

[10] Hu, B., Wang, N., Yu, Z., Cao, Y., Yang, D., and Sun, L. (2021). Optimal Operation of Multiple Energy System Based on Multi-Objective Theory and Grey Theory. *Energies*. 2022, 15, 68. https://doi.org/10.3390/en15010068.

[11] IEEE - Institute of Electrical and Electronics Engineers. (2018). IEEE Standard for Interconnection and Interoperability of Distributed Energy Resources with Associated Electric Power Systems Interfaces. *IEEE Std 1547-2018 (Revision of IEEE Std 1547-2003)*. pp.1-138. doi: 10.1109/IEEESTD.2018.8332112.

[12] Jiang, Y., Li, Y., Tian, Y., and Wang, L. (2018). Phase-Locked Loop Research of Grid-Connected Inverter Based on Impedance Analysis. *Energies*. 11(11):3077. https://doi.org/10.3390/en11113077

[13] Ali Khan, M. Y., Haoming, L., Zhihao, Y., and Xiaoling, Y. (2020). A Comprehensive Review on Grid Connected Photovoltaic Inverters, Their Modulation Techniques, and Control Strategies. *Energies*. volume 13, no. 16: 4185. https://doi.org/10.3390/en13164185

[14] Kraemer, R. A. S., Carati, E. G., da Costa, J. P., Cardoso R., and Stein, C. M. O. (2018). Robust Design of Control Structure for Three-Phase Grid-Tied Inverters. *13th IEEE International Conference on Industry Applications (INDUSCON)*. pp. 636-643, doi: 10.1109/INDUSCON.2018.8627068.

[15] Le, J., Zhao, L., Liao, X., Zhou, Q., and Liang, H. (2021). Stability Analysis of Grid-connected Inverter System Containing Virtual Synchronous Generator under Time Delay and Parameter Uncertainty. *Journal of Electrical Engineering & Technology*. 16(4), 1779–1792. doi:10.1007/s42835-021-00710-y.

[16] Liston Junior, R. A., Carati, E. G., da Costa, J. P., Cardoso, R., and Stein, C. M. O. (2018). Robust Design of Active Damping with Current Estimator for Single-Phase Grid-Tied Inverters. *IEEE Transactions on Industry Applications*. 1–1. doi:10.1109/tia.2018.2838074

[17] Mahlooji, M. H., Mohammadi, H. R., and Rahimi, M. (2018). A review on modeling and control of grid-connected photovoltaic inverters with LCL filter. *Renewable and Sustainable Energy Reviews*. Volume 81, Part 1, 2018, Pages 563-578, ISSN 1364-0321, https://doi.org/10.1016/j.rser.2017.08.002.

[18] Mouton, H. and Putzeys, B. (2012). Understanding the PWM Nonlinearity: Single-Sided Modulation. *IEEE Transactions on Power Electronics*. volume 27. no. 4. pp. 2116-2128. April 2012. doi: 10.1109/TPEL.2011.2169283.

[19] Osorio, C. R. D., Koch, G. G., Pinheiro, H., Oliveira, R. C. L. F., and Montagner, V. F. (2019). Robust Current Control of Grid-Tied Inverters Affected by LCL Filter Soft-Saturation. *IEEE Transactions on Industrial Electronics*. 1–1. doi:10.1109/tie.2019.2938474

[20] Ray, I. (2021). Review of Impedance-Based Analysis Methods Applied to Grid-Forming Inverters in Inverter-Dominated Grids. *Energies*. volume 14. 2686-2703. https://doi.org/10.3390/en14092686

[21] Sayed, M., Ahmed, M., Gamal, M., and Orabi, M. (2014). PWM Control Techniques for Single-Phase Multilevel Inverter Based Controlled DC Cells. *Journal of Power Electronics*. volume 16. 498-511.

[22] Shireen, W., and Kulkarni, R.A.. (2003). Harmonic analysis of three phase PWM inverter systems using MATLAB. *Proceedings of the 2003 American Society for Engineering Education Annual Conference and Exposition*. 10401-10408.

[23] Teodorescu, R., Liserre, M., and Rodriguez, P. (2011). *Grid converters for photovoltaic and wind power systems*. 1 ed - John Wiley and Sons. United Kingdom.

[24] Yang, D., Ruan, X., and Wu, H. (2014). Impedance Shaping of the Grid-Connected Inverter with LCL Filter to Improve Its Adaptability to the Weak Grid Condition. *IEEE Transactions on Power Electronics*. vol. 29, no. 11, pp. 5795-5805, Nov. 2014, doi: 10.1109/TPEL.2014.2300235.

[25] Yang, D., Wang X., and Blaabjerg, F. (2017). Investigation of the sideband effect for the LCL-type grid-connected inverter with high LCL resonance frequency. *IEEE Energy Conversion Congress and Exposition (ECCE)*. 2017. pp. 5601-5606, doi: 10.1109/ECCE.2017.8096932.

[26] Yoon, C., Wang, X., Silva, F. M. F. D., Bak, C. L., and Blaabjerg, F. (2014). Harmonic Stability Assessment for Multi-Paralleled, Grid-Connected Inverters. *Proceedings of the IEEE International Power Electronics and Application Conference and Exposition (IEEE PEAC'14)*. (pp. 1098-1103). IEEE Press. 10.1109/PEAC.2014.7038014

[27] Wang, F., Duarte, J. L., and Hendrix, M. A. M. (2010). Analysis of harmonic interactions between DG inverters and polluted grids. *IEEE International Energy Conference*. pp. 194-199, doi: 10.1109/ENERGYCON.2010.5771674.

[28] Zammit, D., Staines, C. S., and Apap, M. (2014). PR Current Control with Harmonic Compensation in Grid Connected PV Inverters. *International Journal of Electrical, Computer, Energetic, Electronic and Communication Engineering*. volume 8. no 11. 1758-1764.

[29] Zhang, H. and Zhao, Q. (2006). Switching Harmonics in a Three-Phase PWM Inverter. *SAE Technical Papers*. doi: 10.4271/2006-01-3078.